

Measurement of Neutron Whispering Gallery States Using a Pulsed Neutron Beam

G. Ichikawa^{1,2,*} and K. Mishima^{3,1}

¹*High Energy Accelerator Research Organization, Tsukuba 305-0801, Japan*

²*J-PARC Center, Tokai 319-1195, Japan*

³*Kobayashi-Maskawa Institute, Nagoya University, Nagoya 464-8602, Japan*

(Dated: February 28, 2025)

A neutron whispering gallery state is a quantum state localized on a material surface bound by the centrifugal force and the material potential. Precise measurements of such quantum states enable tests of quantum mechanics in non-inertial frames, characterization of the surface potential, and searches for hypothetical short-range interactions at the nanometer scale. We observed a neutron whispering gallery state on a SiO₂ concave mirror using a pulsed cold neutron beam. The measured results agree with theoretical calculations within 1.9% for the centrifugal acceleration $a \approx 7 \times 10^7 \text{ m/s}^2$, which is due to unmodeled deviations of the shape of the concave mirror edge from an ideal one. We found that the sensitivity itself was 1×10^{-4} , which is two orders of magnitude better than the above agreement.

I. INTRODUCTION

General relativity, which describes gravitational interactions, and the Standard Model, which is based on quantum mechanics, explain most physical phenomena and form the foundation of modern physics. However, the unification of these two theories remains an open challenge. Experimental investigations that may provide insights into unification are indispensable. Because general relativity and quantum mechanics describe distinct regimes, only a few experiments test simultaneously. Hence, for several decades, unique physical systems where both gravity and quantum mechanics appear, realized by neutrons, have attracted considerable interest [1, 2].

The Colella-Overhauser-Werner (COW) experiments [1] measured the gravitational phase shift in interference fringes in a silicon single-crystal neutron interferometer. In this setup, the entire interferometer was rotated so that the Earth's gravitational potential introduced a phase difference between the two paths. The initial experiment confirmed that the experimental result roughly agreed with the theoretical prediction, with a discrepancy of about 12%. The primary cause of the discrepancy was the deformation of the interferometer itself when tilted. A subsequent COW-type experiment using two nearly harmonic neutron wavelengths to correct for this deformation improved the agreement with theory to 0.8% [3]. Furthermore, an experiment in which the interferometer was subjected to accelerated motion successfully tested the equivalence of gravity and acceleration with 4% precision, contributing to the verification of the equivalence principle at the quantum level [4], one of the fundamental principles of general relativity.

Gravitationally bound neutron states offer an alternative approach to studying quantum effects in gravity. When the vertical energy of a neutron is below the Fermi potential of a material ($\approx 100 \text{ neV}$), total reflection from a surface forms a state localized to approximately $10 \mu\text{m}$

above the mirror. The gravitationally bound states were first observed using ultracold neutrons [2]. In that experiment, a ceiling designed to remove neutrons was adjusted to different heights while measuring the neutron count. It was confirmed that neutrons survived only when the ceiling height exceeded approximately $15 \mu\text{m}$, corresponding to the extent of the ground-state wave function, which demonstrated the existence of the ground state bound by gravity. Subsequently, the qBOUNCE experiment induced Rabi transitions among these discrete levels with a vibrating floor [5]. Neutrons that transition to higher energy levels are selectively removed by a ceiling, resulting in a marked reduction in the neutron counts at specific transition frequencies. This method allows for precise measurement of the energy-level splitting. It has been demonstrated to achieve a relative precision of 4×10^{-3} against Earth's gravity [6].

These experimental results play an important role in testing gravity and quantum mechanics and, notably, impose unique constraints on theories of gravity beyond general relativity, including noncommutative structures of spacetime [7], the standard-model extension [8], beyond-Riemann gravitational theories [9, 10], and entropic gravity [11–13]. Moreover, because the wave function of gravitationally bound neutrons is localized near the mirror, such experiments can search for hypothetical short-range interactions of the gravitational type [14, 15]. The qBOUNCE experiment [6, 16] also searched for interactions predicted by axions [17] and screened dark energy [18, 19].

Due to the equivalence of gravity and acceleration, quantum states bound by centrifugal force can be regarded as analogs of gravitationally bound states. The quantum states bound by the centrifugal force and a mirror are called neutron whispering gallery states [20]. In an experiment with cold neutrons from a research reactor, interference fringes produced by these states localized to around 100 nm near the mirror surface were observed. Because neutron whispering gallery states undergo hundreds of reflections from the mirror surface in the classical picture, they are highly sensitive to

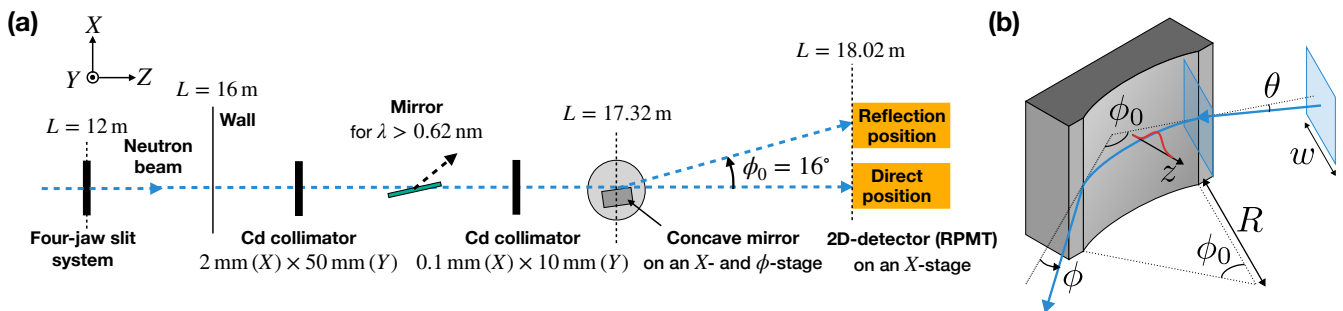


FIG. 1. (a) Schematic top view of the experimental geometry, where L denotes the distance from the neutron moderator. (b) Enlarged view of the concave mirror and the neutron whispering gallery state (red curve). The dimensions and shapes are not drawn to scale. The blue rectangle represents the neutron beam cross section, and the arrow indicates a neutron trajectory. The concave surface has a radius of curvature R and an angular span ϕ_0 . A neutron beam with a width of w enters the mirror at an incidence angle θ , and a neutron becomes bound as a neutron whispering gallery state on the mirror, where z denotes the height from the mirror surface, exiting at a deviation angle ϕ .

the shape of the potential. Therefore, measuring these states can test the surface potential shape and enable searches for hypothetical gravity-like interactions at distances even closer than those accessible by gravitationally bound states. Additionally, by comparing with measurements of gravitationally bound states, one can test the equivalence principle in quantum mechanics [21] and investigate quantum mechanics in non-inertial frames with large accelerations [22].

This paper reports a precise measurement of neutron whispering gallery states using a pulsed neutron beam for the first time. The paper is organized as follows. Section II explains the experimental setup and measurement methods. Section III describes how the radius of curvature and angular span of a concave mirror made of SiO_2 were determined based on surface measurements. In Section IV, we derive the theoretical formalism for neutron whispering gallery states on the concave mirror and show how the observed distributions are calculated. Section V presents the analysis of the experimental data, comparison with theoretical calculations, and discussions. Finally, Section VI provides conclusions and outlook.

II. EXPERIMENT

This experiment was conducted at the low divergence branch of the BL05 beamline [23, 24] of the Materials and Life Science Experimental Facility (MLF) [25] at the Japan Proton Accelerator Research Complex (J-PARC). At J-PARC, a 3 GeV proton beam is directed onto a mercury target at a repetition rate of 25 Hz, generating neutrons through nuclear spallation reactions. Cold neutrons, which have been slowed down by a moderator, are then guided to the beam line. During this experiment, the facility was operated at a beam power of approximately 700 kW.

A schematic top view of the apparatus used in this experiment is shown in Fig. 1(a). In the following description, the distance from the neutron moderator is denoted

by L and the components are explained from upstream to downstream along the beamline. The cold neutron beam delivered to the beamline is first shaped by a four-jaw slit system located at $L = 12$ m. In this experiment, the horizontal beam width (the X direction in the figure) was fixed at 6 mm, providing in a horizontal divergence with a standard deviation of 0.09 mrad. The vertical beam width (the Y direction in the figure) was set to 44 mm, which results vertical divergence of 5 mrad.

The beam travels through a vacuum guide tube up to $L = 16$ m. A Cd collimator with an opening of 2 mm (X) \times 50 mm (Y) was placed at $L = 16.49$ m, and a neutron mirror that reflects and removes neutrons with wavelength $\lambda > 0.62$ nm was positioned at $L = 17.04$ m to prevent detection of delayed neutrons from the previous pulse. A second Cd collimator with an opening of 0.1 mm (X) \times 10 mm (Y) was placed at $L = 17.17$ m. This final collimator defined the beam size entering the concave mirror. A glass concave mirror mounted on an X - and ϕ -stages (ϕ denotes yaw-rotation) was placed at $L = 17.32$ m. Floor vibrations were suppressed by an active vibration isolation table. The concave mirror was made of OHARA QUARTZ SK-1300B (SiO_2 , density 2.2 g/cm³, surface potential $U_0 = 90.5$ neV), and its concave surface was fabricated via magneto-rheological finishing by Crystal Optics Inc. with high precision. A 15 mm \times 25 mm \times 40 mm rectangular piece of glass had one of its 25 mm \times 40 mm faces formed into a concavity about the long edge as an axis.

An expanded view of the concave mirror and the relevant parameters used in this experiment are shown in Fig. 1(b). A portion of the incoming neutron beam is bound by the material potential and the centrifugal potential, forming a whispering gallery state that travels along the mirror surface. The beam direction is bent by the angular span ϕ_0 of the concave mirror. Other parameters are: R , the radius of curvature of the concave mirror; w , the beam width; θ , the incidence angle of the beam relative to the mirror's tangential direction; z , the height from the mirror surface toward the

center of curvature; and ϕ , the deviation angle of the outgoing neutrons. The concave mirror was designed with a radius of curvature $R = 25$ mm and an angular span $\phi_0 = 16^\circ$. The radius of curvature and angular span were measured by a three-dimensional profilometer (UA3P, Panasonic). Details of the measurement procedure are presented in Section III. The average surface roughness (R_a) was measured by a three-dimensional optical surface profiler (NewView, Zygo) over an area of 0.08 mm \times 0.08 mm, giving $R_a = 0.58$ nm.

A two-dimensional detector with time resolution, utilizing a resistance-division photomultiplier tube (RPMT) [26], on an X -stage was placed at $L = 18.02$ m. The neutron whispering gallery state was observed as the distribution of λ and ϕ on the RPMT, measured at a position where the RPMT was shifted 199 mm in the $+X$ direction. We defined a foreground region of 30 mm (X) \times 21 mm (Y) on the RPMT plane and background regions of 30 mm (X) \times 10.5 mm (Y) above and below the foreground region for the neutron whispering gallery measurement.

During neutron whispering gallery measurements, after ensuring that the neutron beam was incident on the entrance of the concave surface by adjusting the X - and ϕ -stages, the rotation angle of the concave mirror was scanned in 0.03° increments at five points, each measured for 5 hours, to find the angle that maximized neutron counts. The angle with the highest neutron count was used for the analysis of the neutron whispering gallery state. To compare with the theoretical curve, the wavelength distribution of neutrons directly incident on the detector without the concave mirror was measured and used as a normalization. In that reference measurement, the vertical beam width was reduced to 4 mm to avoid detector pileup. To reproduce an effective 44 mm opening, we shifted the 4 mm beam eleven times across the full span, and all data were summed to obtain the final distribution.

III. GEOMETRY OF CONCAVE MIRROR

This section describes how to determine the radius of curvature R and the angular span ϕ_0^{surf} of the concave mirror from surface measurements. Figures 2(a)–(c) show the three-dimensional profile measurement of the mirror surface. We defined the measurement plane as $X_{\text{surf}}Y_{\text{surf}}$ and measured the height Z_{surf} of the glass surface to obtain the concave shape. The surface was scanned along the X_{surf} axis every 2 mm in the Y_{surf} direction. Here, $Y_{\text{surf}} = 0$ corresponds to the center of the region hit by the neutron beam. In this experiment, we aligned the Y axis of Fig. 1(a) with the Y_{surf} axis of the surface measurement, so that the neutron beam entered from the $+X_{\text{surf}}$ side.

Figures 2(d)–(f) plot the deviations of the surface measurement data from a circular fit for each scan line. The deviations are defined as negative if the surface lies out-

side (farther from the center) than the fitted circle. The X_{surf} coordinates are converted to ϕ_{surf} , the angular coordinate on the mirror surface. We fit the obtained radii R with a linear function of Y_{surf} and evaluate the change in R between $Y_{\text{surf}} = -6$ mm and 6 mm, which corresponds to the region illuminated by the neutron beam, as an uncertainty. This yields $R = 25.168(8)$ mm.

Figures 2(g)–(i) show the slope of the surface profile, obtained by converting deviations from the ideal circular fit into slope angles. We determine the angular span of the mirror ϕ_0^{surf} by defining the region where the absolute value of the slope does not exceed a threshold θ_{thr} . The angular span is given by $\phi_0^{\text{surf}} = \phi_{\text{max}}^{\theta_{\text{thr}}} - \phi_{\text{min}}^{\theta_{\text{thr}}}$, where θ_{thr} is the positive threshold angle, and $\phi_{\text{min}}^{\theta_{\text{thr}}}$ ($\phi_{\text{max}}^{\theta_{\text{thr}}}$) is the surface position in the vicinity of the mirror edge in Figs. 2(h) or (i) where the slope graph crosses θ_{thr} ($-\theta_{\text{thr}}$). In Figs. 2(h) and (i), the data at $Y_{\text{surf}} = 6$ mm are shown as an example. The threshold angle θ_{thr} was determined according to the deviation angle ϕ presented in Section V. Specifically, the neutron whispering gallery distribution first appears at $\lambda = 0.26$ nm, and neutrons with wavelengths up to $\lambda = 0.62$ nm where neutrons pass through the upstream mirror unfiltered. We took the corresponding classical cutoff angles of 2.7 mrad (for 0.26 nm) and 6.5 mrad (for 0.62 nm) as the thresholds θ_{thr} . Using these thresholds, the averages and standard deviations of the angular span were obtained as $15.850(18)^\circ$ and $15.8603(18)^\circ$, respectively. We adopted their average as $\phi_0^{\text{surf}} = 15.86(2)^\circ$.

IV. FORMALISM

In this section, we formulate the neutron whispering gallery state based on quantum mechanics [27] and derive the ideal distribution observed in our experiment. In cylindrical coordinates near the mirror surface, ignoring the axial parameter due to the trivial symmetry, the one-dimensional Schrödinger equation can be written as

$$\left[-\frac{\hbar^2}{2m} \frac{d^2}{dz^2} + U_0 \Theta(-z) + \frac{mv^2z}{R} - E_n \right] \psi_n(z) = 0, \quad (1)$$

where \hbar is the reduced Planck constant, m is the neutron mass, z is the displacement from the mirror surface toward the center of curvature, $U_0 = 90.5$ neV is the optical potential of SiO_2 , Θ is the Heaviside step function indicating the region of the mirror, R is the radius of curvature, v is the neutron velocity, n is the principal quantum number, E_n is the radial energy, and ψ_n is the wave function. The third term on the left side corresponds to the centrifugal potential maz due to the centrifugal acceleration $a = v^2/R$. Although ψ_n or E_n depends on v (or λ), here we omit explicit notation of v .

We define the characteristic length, energy, momentum, and time scales for this system as

$$z_0 = \left(\frac{\hbar^2}{2m^2a} \right)^{1/3}, \quad E_0 = maz_0 = \left(\frac{ma^2\hbar^2}{2} \right)^{1/3}, \quad (2)$$

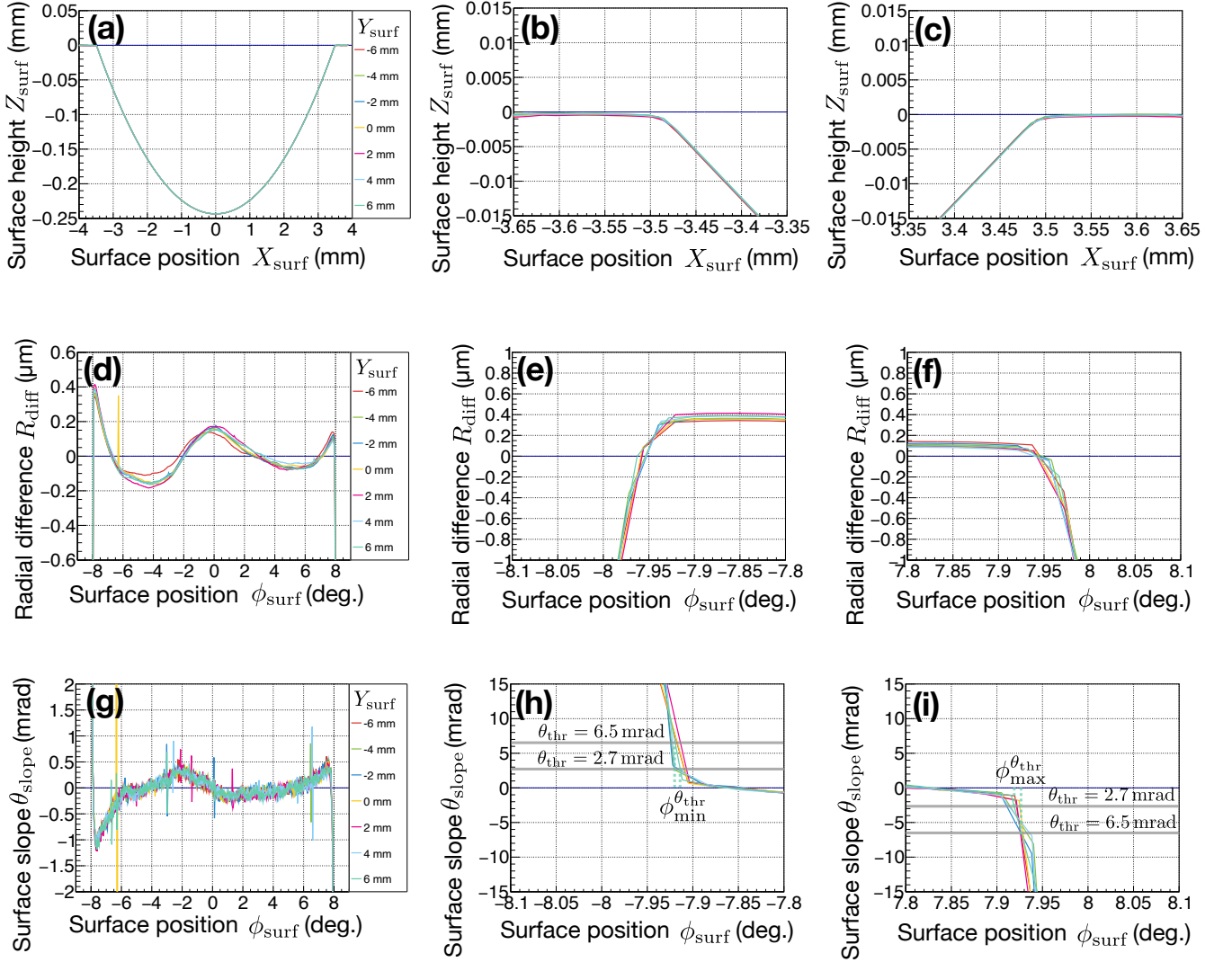


FIG. 2. Surface metrology data of the concave mirror. (a)–(c) show the three-dimensional surface profiles; (d)–(f) show the deviations from the circular fits; (g)–(i) show the slope angles derived from these deviations. (a), (d), and (g) cover the entire concave surface, while the others provide magnified views of the edges. The angle values $\phi_{\text{min}}^{\theta_{\text{thr}}}$ and $\phi_{\text{max}}^{\theta_{\text{thr}}}$ are used to determine the mirror’s angular span; (h) and (i) show an example at $Y_{\text{surf}} = 6$ mm.

$$p_0 = \sqrt{2mE_0}, \quad t_0 = \hbar/E_0. \quad (3)$$

By normalizing z and E_n as $\zeta = z/z_0$ and $\epsilon_n = E_n/E_0$, respectively, Eq. (1) becomes

$$\left[-\frac{d^2}{d\zeta^2} + u\Theta(-\zeta) + \zeta - \epsilon_n \right] \psi_n(\zeta) = 0, \quad (4)$$

where $u = U_0/E_0$, and ψ_n is redefined for the dimensionless variable. Examples of numerically computed eigenfunctions and eigenenergies for $R = 25$ mm at $\lambda = 0.3$ nm and 0.5 nm are shown in Fig. 3. Each eigenstate is quasi-stable due to tunneling into the region $z < 0$; thus its eigenenergy can be written as $\epsilon_n = \beta_n - i\gamma_n$, where β_n is the real part and γ_n is the imaginary part. As shown in Fig. 3, the slope of the centrifugal potential varies with the neutron wavelength, and the number of surviving states increases as the wavelength increases.

When a single neutron enters the mirror edge, the wave function is

$$\Psi(\zeta, \tau = 0) = \sum_n a_n \psi_n(\zeta), \quad (5)$$

where $\tau = t/t_0$ is the dimensionless time elapsed after incidence on the mirror, and a_n is the complex coefficient giving the weight and phase of each eigenstate. Immediately before incidence on the mirror edge, the neutron can be treated as a monochromatic wave in the radial direction, since the angular divergence of the beam (0.09 mrad) is much smaller than the divergence of the whispering gallery state (see Section V). The dimensionless radial momentum can be written as $\xi_\theta = -mv \sin \theta / p_0$ using the incidence angle θ . Because only the region near the mirror surface contributes to forming the whispering gallery state and the component

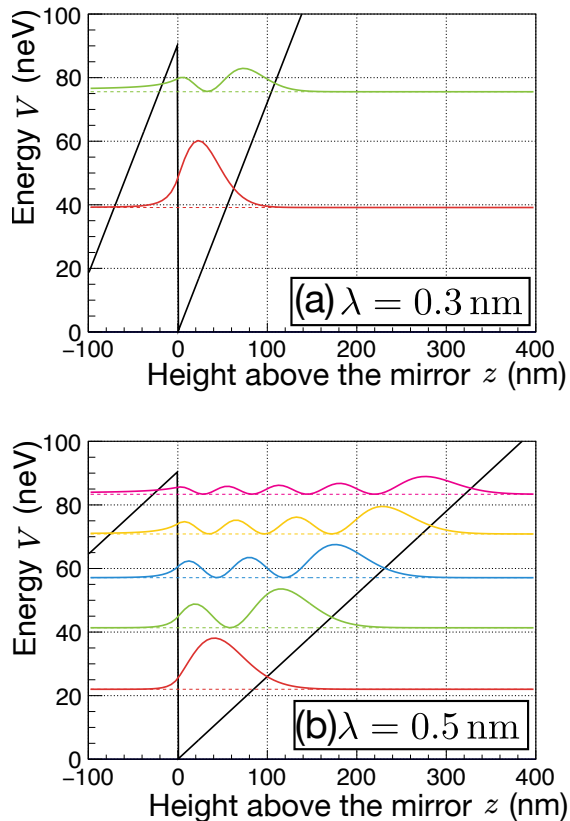


FIG. 3. Eigenfunctions and eigenenergies of neutron whispering gallery states for $\lambda = 0.3$ nm (a) and 0.5 nm (b). The horizontal axis is z , the displacement from the mirror surface toward the center of curvature, and the vertical axis is energy. The black solid line is the sum of the mirror optical potential and the centrifugal potential, the horizontal dotted lines show the real part of each eigenenergy, and the curves represent the absolute squares of the corresponding eigenfunctions. Only bound states with real eigenenergies below the mirror potential are plotted.

directly entering $\zeta < 0$ is refracted and does not form a bound state, we can set the beam width region as $0 \leq \zeta < l = w/z_0$. Then, the incident wave function is written as

$$\psi_\theta(\zeta) = \begin{cases} \exp(i\zeta\xi_\theta)/\sqrt{l} & 0 \leq \zeta < l \\ 0 & \text{otherwise.} \end{cases} \quad (6)$$

By assuming the continuity of the wave function at the mirror entrance, we have

$$a_n = \int_0^l \psi_n^*(\zeta) \psi_\theta(\zeta) d\zeta. \quad (7)$$

The wave function at the mirror exit is given by the time evolution of Eq. (5):

$$\Psi(\zeta, \tau_0) = \sum_n c_n \psi_n(\zeta) \exp(-i\beta_n \tau_0), \quad (8)$$

where $\tau_0 = (R\phi_0/v)/t_0$ and $c_n = a_n \exp(-\gamma_n \tau_0)$. In this experiment, we measured the deviation angle ϕ , so we

must consider the momentum eigenfunctions φ_n related to ψ_n by Fourier transformation. The momentum-space wave function at the exit is

$$\Phi(\xi, \tau_0) = \sum_n c_n \varphi_n(\xi) \exp(-i\beta_n \tau_0), \quad (9)$$

where $\xi = mv_r/p_0$ is the dimensionless radial momentum and v_r is the radial velocity. Using the relation of the deviation angle $\phi = \arctan(v_r/v)$, the probability distribution of λ and ϕ is

$$\begin{aligned} P(\lambda, \phi) &= |\Phi(\xi_\phi, \tau_0)|^2 \\ &= \sum_n |c_n|^2 |\varphi_n(\xi_\phi)|^2 \\ &\quad + \sum_{n \neq m} c_m^* c_n \varphi_m^*(\xi_\phi) \varphi_n(\xi_\phi) \exp[-i(\beta_n - \beta_m) \tau_0], \end{aligned} \quad (10)$$

where $\xi_\phi = 2\pi\hbar \tan \phi / (p_0 \lambda)$ and $\tau_0 = R\phi_0 m \lambda / (2\pi\hbar t_0)$.

V. ANALYSIS

The data obtained from the neutron whispering gallery measurements were normalized by the wavelength distribution measured without the concave mirror and then compared with the theoretical distribution. Figures 4(a) and (b) show the λ - ϕ two-dimensional histograms of the observed and theoretical distributions of the neutron whispering gallery.

The wavelength λ was obtained from the time-of-flight T , neutron mass m , and flight distance L_F as $\lambda = T / (2\pi\hbar m L_F)$, with a high-precision correction measured by Bragg reflections [28]. Due to neutron moderation, the wavelength distribution measured by the time-of-flight method appears 0.8% longer than the actual wavelength. Additionally, the neutron wavelengths detected at a certain time are subject to broadening with a standard deviation of 0.8%. Hence, the distribution $P(\lambda, \phi)$ in Eq. (10) was convoluted with a Gaussian function of width 0.008λ .

The deviation angle ϕ was defined as the difference between the measured scattering angle and the mean scattering angle corresponding to ϕ_0 . The angular span ϕ_0 can be determined not only from surface measurements but also from the neutron scattering angle, and the value obtained by this method is defined as ϕ_0^{geom} . We determined ϕ_0^{geom} using the $0.30 \text{ nm} \leq \lambda < 0.35 \text{ nm}$ region of the whispering gallery measurement which corresponds to the ground state. Then, we obtained $\phi_0^{\text{geom}} = 16.06(2)^\circ$. The value ϕ_0^{geom} differs by 1.3% from the surface-measurement value of $\phi_0^{\text{surf}} = 15.86(2)^\circ$, exceeding their stated systematic uncertainty. This discrepancy likely arises from the fact that the mirror surface is slightly different from the ideal concavity near its edges, allowing the neutron wave function to follow the surface shape and scatter to a larger angle in a manner not fully accounted for in our calculation.

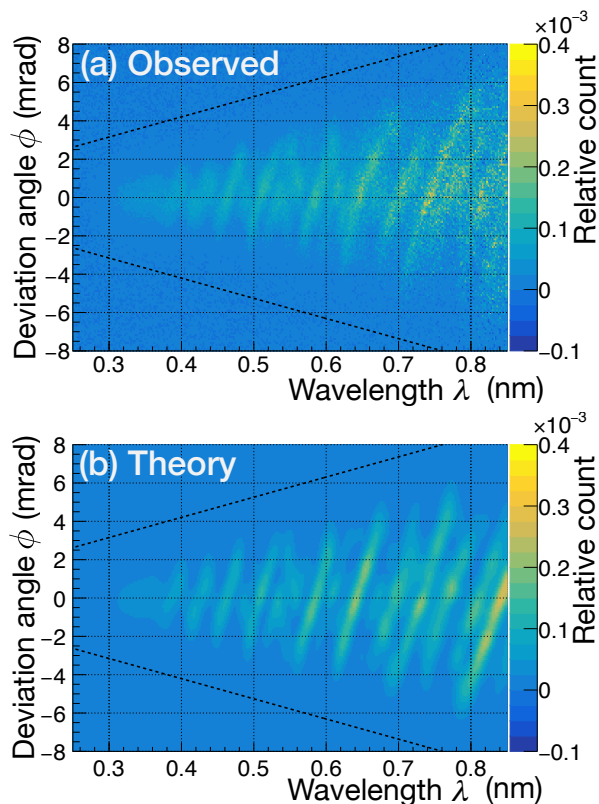


FIG. 4. (a) Observed and (b) theoretical two-dimensional distributions of neutron whispering gallery as functions of λ and ϕ . The bin sizes are 0.002 nm and 0.1 mrad, respectively. The diagonal dotted line corresponds to the classical cutoff angle defined by the mirror potential energy. The theory plot shown includes the additional loss term and best-fit parameters described in the text.

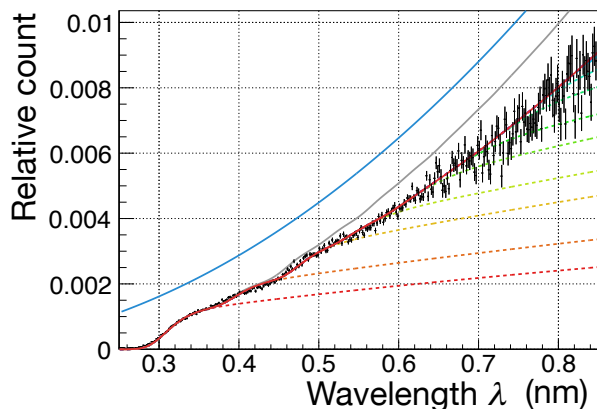


FIG. 5. Wavelength distribution of the neutron whispering gallery. Black data points represent the measured data, while the blue curve corresponds to the classical theory, the gray curve is the quantum theory without additional losses, and the red curve is the quantum theory including additional losses. The colored dashed lines illustrate the contribution of $n \leq 1, 2, \dots$ states to the red curve. The theoretical curves use best-fit parameters.

Figure 5 shows the wavelength distribution obtained by projecting the neutron whispering gallery data onto the λ axis. We used $\phi_0^{\text{geom}} = 16.06^\circ$ for the theoretical calculation here. The rising edge at $\lambda = 0.26$ nm, corresponding to the mirror potential $U_0 = 90.5$ neV, and the staircase-like increase due to the increasing number of bound states are in good agreement between experiment and quantum theory. However, the measured counts are lower than the theoretical curve at longer wavelengths, suggesting a wavelength-dependent neutron loss from the bound states.

It is known that neutron reflection at the surface potential typically leads to a loss of about 10^{-4} per bounce [29], which does not reproduce the data here because the loss would become larger at shorter wavelengths, opposite to the observed behavior. If the material surface contains impurities, the potential near the floor is effectively a sigmoidal “soft potential” [30], reducing the reflectivity. However, such a soft potential significantly shifts the rise at $\lambda = 0.26$ nm in Fig. 5 and the interference fringes in Fig. 4, failing to match our data. A classical model where the radial energy of the neutron changes from the reflection of a tilted floor also fails to reproduce the data because the resulting energy shift changes the position of the interference fringes.

The fact that more levels exist below U_0 in the longer wavelength region as illustrated in Fig. 3 suggests that the additional loss occurs for levels with larger n . To achieve such an effect, we introduced an additional loss model in which the mirror potential height fluctuates by Δ , for example, due to surface roughness or waviness, so that neutrons sometimes experience a reduced potential and escape the bound state upon reflection. In a classical picture, for the n -th bound state with a reflection period

$$t_{\text{ref}} = \frac{2}{a} \sqrt{\frac{2E_n}{m}}, \quad (11)$$

if the floor potential height fluctuates by Δ , the probability that a neutron in the n -th state is lost per unit time t_0 is

$$\mu_n = \frac{t_0}{t_{\text{ref}}} \left[\int_{U_0 - E_n}^{\infty} dE \frac{k}{\sqrt{2\pi\Delta}} \exp\left(-\frac{E^2}{2\Delta^2}\right) \right], \quad (12)$$

where k is the loss coefficient. Thus, the coefficient c_n in Eq. (5) becomes

$$c'_n = c_n \exp(-\mu_n \tau_0). \quad (13)$$

We fit the theoretical wavelength distribution, including this additional loss, to the data (Fig. 5). The fit parameters are θ , w , k , and Δ . Here, w determines the overall normalization by setting the phase-space density of the beam. The fit excludes $\lambda > 0.62$ nm, which is removed by the filter mirror. The best-fit results are $\theta = -0.01(1)$ mrad, $w = 77.5(5)$ μm , $k = 1.4(9)$, $\Delta = 12(1)$ neV, indicating that the mirror potential effectively fluctuates by about 13% relative to U_0 on reflection.

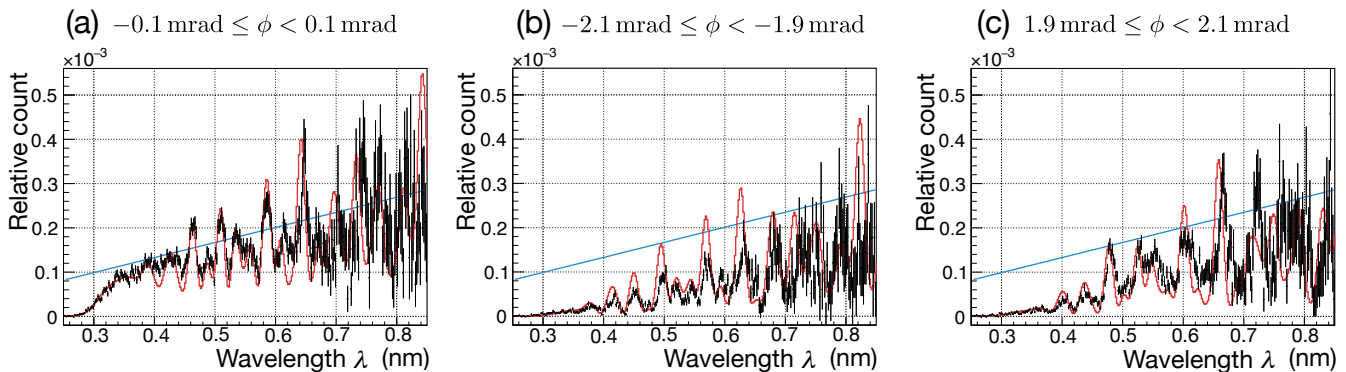


FIG. 6. Wavelength distributions for (a) $-0.1 \text{ mrad} \leq \phi < 0.1 \text{ mrad}$, (b) $-2.1 \text{ mrad} \leq \phi < -1.9 \text{ mrad}$, and (c) $1.9 \text{ mrad} \leq \phi < 2.1 \text{ mrad}$. The black points represent the experimental data, the blue curves denote the classical calculation, and the red curves correspond to the quantum model including additional losses. The interference fringes were fitted under the condition in (a), and the same best-fit parameters are used in (b) and (c).

One can exploit the interference fringes more fully by examining the shape of the fringes in two-dimensional λ - ϕ space. In Fig. 6(a), we compare the wavelength distribution in the region $|\phi| < 0.1 \text{ mrad}$ between experiment and theory. We treat the angular span of the mirror ϕ_0 as a fit parameter. Fitting yields $\phi_0^{\text{fit}} = 16.004(1)^\circ$, intermediate between ϕ_0^{surf} and ϕ_0^{geom} . Figures 6(b) and (c) show the wavelength distributions near $\phi = \pm 2 \text{ mrad}$ using the fit result. In the negative-angle region of $-2.1 \text{ mrad} \leq \phi < -1.9 \text{ mrad}$, the measured neutron counts are lower than the theoretical prediction, likely because the mirror surface extends even beyond ϕ_0 near the edge so that neutrons with $\phi < 0$ (indicating motion in the $-z$ direction) lose intensity upon reflection of the mirror.

The angular span of the concave mirror was determined using three different methods: surface measurement, geometric analysis, and interference fringe fitting. The values obtained from these methods agreed to within 1.3%: $\phi_0^{\text{surf}} = 15.86(2)^\circ$, $\phi_0^{\text{geom}} = 16.06(2)^\circ$, and $\phi_0^{\text{fit}} = 16.003(2)^\circ$. Their discrepancy exceeds each stated systematic uncertainty but is still within 1.3%. This correspondence translates to 1.9% for the centrifugal acceleration a and 1.3% for the energy scale E_0 because the interference pattern is determined by $E_0 R \phi_0 / v \propto E_0 \phi_0$ and the energy scale is $E_0 \propto a^{2/3}$. Fitting of the interference fringes inside $|\phi| < 0.1 \text{ mrad}$ suggests an ideal sensitivity of 8×10^{-5} to ϕ_0 for a 5-hour measurement, or two orders of magnitude better than the present analysis. This corresponds to a potential sensitivity of 1×10^{-4} for a and E_0 , which is better than the current precision of gravitationally bound states [6]. This sensitivity can be achieved if the angular span and the curvature radius of the mirror and the neutron wavelength are determined with sufficient precision and if the effects of the concave edge are accurately modeled.

VI. CONCLUSION AND PROSPECTS

We conducted a neutron whispering gallery experiment by utilizing a pulsed cold neutron beam at J-PARC onto a precisely polished glass concave mirror and observing the bound state with a two-dimensional, time-resolving detector. We found good agreements between data and theory in the wavelength distribution by introducing an additional loss mechanism where the mirror potential height fluctuates, causing neutrons to leave the bound state. Three independent determinations of the angular span of the mirror gave $\phi_0^{\text{surf}} = 15.86(2)^\circ$, $\phi_0^{\text{geom}} = 16.06(2)^\circ$, and $\phi_0^{\text{fit}} = 16.003(2)^\circ$. They agree within 1.3%, exceeding their stated systematic uncertainties but consistent at that level. We interpret the discrepancy as arising from unmodeled deviations of the shape of the mirror edge from an ideal one. This agreement of 1.3% corresponds to verification at 1.9% for the centrifugal acceleration a and 1.3% for the energy scale of the whispering gallery state E_0 . Our analysis of the interference fringes suggests that the sensitivity could be improved to 1×10^{-4} which exceeds the current sensitivity of the Earth's gravitational bound state if the angular span and the curvature radius of the mirror, and the neutron wavelength can be known more precisely and the effect of the concave edge can be correctly calculated.

For future improvements, by measuring the phase-space density of the beam independently with a high-precision collimator system, the uncertainty associated with w can be eliminated. The effects of a rounded mirror edge could be more precisely calculated by simulating wave-packet evolution under a time-dependent potential boundary. Regarding additional losses, one might minimize them by using a mirror with extremely low surface roughness or examining multiple samples with different surface conditions to identify the physical origin of the potential height fluctuations. Furthermore, by detecting short-lived components that penetrate the mirror [27], it is possible to determine whether the additional loss is due

to penetration or reflection from the mirror. Searching for hypothetical short-range interactions with a range of about 10 nm beyond the current limit [31, 32] requires a precision of about 1×10^{-5} in E_0 . To achieve that, it may be necessary to measure detailed structures in the wave function such as the classical period of motion or the quantum revival period [33] of the neutron traveling on the mirror with a monochromatic neutron beam.

ACKNOWLEDGMENTS

We would like to thank N. Naganawa and Y. Nambu of Nagoya University for fruitful discussions on equivalence principles. This research was supported by JSPS KAKENHI Grant Numbers 21K03594 and 24K07083. The neutron experiment at the Material and Life Science Experimental Facility of the J-PARC was performed under user programs (Proposal Nos. 2021B0141, 2022A0204, and 2022B0327) and an S-type project of KEK (Proposal No. 2019S03).

* Corresponding author: go.ichikawa@kek.jp

- [1] R. Colella, A. W. Overhauser, and S. A. Werner, Observation of Gravitationally Induced Quantum Interference, *Phys. Rev. Lett.* **34**, 1472 (1975).
- [2] V. V. Nesvizhevsky, H. G. Börner, A. K. Petukhov, H. Abele, S. Baeßler, F. J. Rueß, T. Stöferle, A. Westphal, A. M. Gagarski, G. A. Petrov, and A. V. Strelkov, Quantum states of neutrons in the Earth's gravitational field, *Nature* **415**, 297 (2002).
- [3] K. C. Littrell, B. E. Allman, and S. A. Werner, Two-wavelength-difference measurement of gravitationally induced quantum interference phases, *Phys. Rev. A* **56**, 1767 (1997).
- [4] U. Bonse and T. Wroblewski, Measurement of Neutron Quantum Interference in Noninertial Frames, *Phys. Rev. Lett.* **51**, 1401 (1983).
- [5] T. Jenke, P. Geltenbort, H. Lemmel, and H. Abele, Realization of a gravity-resonance-spectroscopy technique, *Nature Physics* **7**, 468 (2011).
- [6] G. Cronenberg, P. Brax, H. Filter, P. Geltenbort, T. Jenke, G. Pignol, M. Pitschmann, M. Thalhammer, and H. Abele, Acoustic Rabi oscillations between gravitational quantum states and impact on symmetron dark energy, *Nat. Phys.* **14**, 1022 (2018).
- [7] A. Saha, Colella-overhauser-werner test of the weak equivalence principle: A low-energy window to look into the noncommutative structure of space-time?, *Phys. Rev. D* **89**, 025010 (2014).
- [8] C. A. Escobar, A. Martín-Ruiz, A. M. Escobar-Ruiz, and R. Linares, Testing the scalar sector of the standard-model extension with neutron gravity experiments, *The European Physical Journal Plus* **137**, 1186 (2022).
- [9] V. A. Kostelecký and Z. Li, Searches for beyond-riemann gravity, *Phys. Rev. D* **104**, 044054 (2021).
- [10] A. Ivanov, M. Wellenzohn, and H. Abele, Quantum gravitational states of ultracold neutrons as a tool for probing of beyond-Riemann gravity, *Physics Letters B* **822**, 136640 (2021).
- [11] E. Verlinde, On the origin of gravity and the laws of Newton, *Journal of High Energy Physics* **2011**, 29 (2011).
- [12] M. Chaichian, M. Oksanen, and A. Tureanu, On gravity as an entropic force, *Physics Letters B* **702**, 419 (2011).
- [13] A. J. Schimmoller, G. McCaul, H. Abele, and D. I. Bondar, Decoherence-free entropic gravity: Model and experimental tests, *Phys. Rev. Res.* **3**, 033065 (2021).
- [14] J. Murata and S. Tanaka, A review of short-range gravity experiments in the LHC era, *Classical Quantum Gravity* **32**, 033001 (2015).
- [15] S. Sponar, R. P. Sedmik, M. Pitschmann, H. Abele, and Y. Hasegawa, Tests of fundamental quantum mechanics and dark interactions with low-energy neutrons, *Nat. Rev. Phys.* **3**, 309 (2021).
- [16] T. Jenke, G. Cronenberg, J. Burgdörfer, L. A. Chizhova, P. Geltenbort, A. N. Ivanov, T. Lauer, T. Lins, S. Rotter, H. Saul, U. Schmidt, and H. Abele, Gravity resonance spectroscopy constrains dark energy and dark matter scenarios, *Phys. Rev. Lett.* **112**, 151105 (2014).
- [17] J. E. Moody and F. Wilczek, New macroscopic forces?, *Phys. Rev. D* **30**, 130 (1984).
- [18] J. Khoury and A. Weltman, Chameleon cosmology, *Phys. Rev. D* **69**, 044026 (2004).
- [19] K. Hinterbichler and J. Khoury, Screening long-range forces through local symmetry restoration, *Phys. Rev. Lett.* **104**, 231301 (2010).
- [20] V. V. Nesvizhevsky, A. Y. Voronin, R. Cubitt, and K. V. Protasov, Neutron whispering gallery, *Nat. Phys.* **6**, 114 (2010).
- [21] M. Zych and Č. Brukner, Quantum formulation of the Einstein equivalence principle, *Nat. Phys.* **14**, 1027 (2018).
- [22] M. Nauenberg, Einstein's equivalence principle in quantum mechanics revisited, *Am. J. Phys.* **84**, 879 (2016).
- [23] K. Mishima *et al.*, Design of neutron beamline for fundamental physics at J-PARC BL05, *Nucl. Instrum. Methods Phys. Res., Sect. A* **600**, 342 (2009).
- [24] K. Mishima, J-PARC Neutron Beam Line (BL05/NOP) for Fundamental Physics, *Hamon* **25**, 156 (2015).
- [25] K. Nakajima, Y. Kawakita, S. Itoh, J. Abe, K. Aizawa, H. Aoki, H. Endo, M. Fujita, K. Funakoshi, W. Gong, *et al.*, Materials and Life Science Experimental Facility (MLF) at the Japan Proton Accelerator Research Complex II: Neutron Scattering Instruments, *Quantum Beam Sci.* **1**, 9 (2017).
- [26] K. Hirota, T. Shinohara, K. Ikeda, K. Mishima, T. Adachi, T. Morishima, S. Satoh, T. Oku, S. Yamada, H. Sasao, J.-i. Suzuki, and H. M. Shimizu, Development of a neutron detector based on a position-sensitive photomultiplier, *Phys. Chem. Chem. Phys.* **7**, 1836 (2005).
- [27] V. V. Nesvizhevsky, R. Cubitt, K. V. Protasov, and A. Y. Voronin, The whispering gallery effect in neutron scattering, *New J. Phys.* **12**, 113050 (2010).
- [28] H. E. Shimizu, Precise measurement of ^3He absorption cross sections for neutrons using the J-PARC pulsed neutron source, in *Proceedings of the J-PARC Symposium*

- 2024 (2024) [to be published].
- [29] L. Koester and A. Steyerl, *Neutron Physics* (Springer Berlin, Heidelberg, 1977) pp. 91–110.
- [30] H. Scheckenhofer and A. Steyerl, Diffraction and Mirror Reflection of Ultracold Neutrons, *Phys. Rev. Lett.* **39**, 1310 (1977).
- [31] B. Heacock, T. Fujiie, R. W. Haun, A. Henins, K. Hirota, T. Hosobata, M. G. Huber, M. Kitaguchi, D. A. Pushin, H. Shimizu, M. Takeda, R. Valdillez, Y. Yamagata, and A. R. Young, Pendellösung interferometry probes the neutron charge radius, lattice dynamics, and fifth forces, *Science* **373**, 1239 (2021).
- [32] B. W. Harris, F. Chen, and U. Mohideen, Precision measurement of the Casimir force using gold surfaces, *Phys. Rev. A* **62**, 052109 (2000).
- [33] R. Robinett, Quantum wave packet revivals, *Phys. Rep.* **392**, 1 (2004).